SUPPORTING INFORMATION APPENDIX

SI Results. ***cMyBP-C site-directed mutagenesis, labeling and phosphorylation.*** We determined that the C0C2 fragment of cMyBP-C (WT C0-C2) contains a single Cys (C248) that is readily labeled by maleimide-group fluorescent dyes and spin labels, whereas the other 4 Cys in C0C2 are not readily labeled under our labeling conditions. Therefore, we introduced a second reactive Cys to replace a surface accessible Ser residue either in the C0, C1, or C2 domain (S18C, S169C, or S440C) in the three varieties of double-Cys mutants used in this study. Site-directed mutagenesis was confirmed by DNA sequence analysis. C0C2 was expressed in BL-21 cells and purified by His-affinity nickel resin and further purified by size exclusion chromatography (>95% purity). For FRET experiments, the extent of labeling was confirmed by UV spectrophotometry, colorimetric protein assay, and mass spectrometry. These values were used to constrain the fits of TR-FRET analysis. The molar ratio of IAEDANS labeling (donor) [1,5-IAEDANS, 5-((((2-Iodoacetyl)amino)ethyl)amino)Naphthalene-1-Sulfonic Acid] (Molecular Probes) per Cys labeling site in double-Cys C0C2 was determined to be 9-22% and 72-89% for FMal labeling (acceptor) [Fluorescein-5-maleimide] (Molecular Probes) per Cys labeling site. The extent of MSL labeling [N-(1-Oxyl-2,2,6,6-tetramethyl-4-piperidinyl)maleimide] (Toronto Research Chemicals) was to near completion, as determined by spin-counting using a Bruker E500 spectrometer at X-band (9.5 GHz) with an SHQ cavity at a microwave power where there was no saturation (0.03 mW). The molar ratio of spin labels per labeling site was determined to be 0.96 ± 0.04.

Short distance examination within C1 domain of C0C2 (S169C.C248) using CW-EPR. Continuous-wave (CW) dipolar EPR (most sensitive to spin-spin distances <2.5 nm) was used to measure between two maleimide spin labels (MSL-MSL). Detected distances were estimated to be just beyond the instrument sensitivity (i.e., 2.6-2.7 nm distances are weakly detectable), confirming that DEER spectroscopy is most suitable for studying our set of intra- and inter- domain probe pairs that we engineered in C0C2. Indeed, a similar distance ~2.6 nm was detected using both CW-EPR and DEER. However, with DEER having sensitivity beyond 2.5 nm, with excellent resolution for both distance and disorder measurements between 2 and 6 nm, the statistical confidence of the FWHM is much better for DEER as compared to CW-EPR for these probe sites (Tables S1 and S2). For example, using CW-EPR analysis of the spin labeled C0C2 (S169C.C248) within C1 (Fig. S1), we observed a small but significant difference in the line-width of ~0.6G, which correlates to a measured distance of ~2.6 nm and fairly high disorder ~2 nm, due to the long distance sensitivity limit for CW-EPR (optimal for distances <2.5 nm); using DEER (and FRET), this FWHM is more realistic for an Ig-like domain at 0.3-0.6 nm. Thus, DEER is the dipolar EPR method of choice for studying structure and dynamics in our set of doubly-labeled C0C2 (within the C1 domain, across PAL, or across MyBP-C motif).

DEER and FRET analyses comparison. Intra-C1 domain and motif-flanking C0C2 distances distributions using DEER and FRET were determined to be very similar in comparison and nearly superimposable (main text Fig. 2C and Fig. S2), whereas PAL-flanking measurements yielded qualitatively similar broad distributions to suggest significant molecular disorder for the open conformation (FWHM ~2 nm), consistent with other structural studies [1]. Both DEER and FRET analyses for C0C2 mutants indicate that the data is best fit to a sum of two Gaussian distance distributions. For FRET analysis, the donor-only lifetimes were best fit to three exponentials (Fig. S3) and the donor-acceptor lifetimes were best fit to two Gaussians (Fig. S4). Distance distributions for all three constructs with and without PKA treatment are summarized in Fig. S5. For DEER analysis, the decays were background-subtracted and similarly fit to one or two Gaussians (Fig. S6), with the two-Gaussian giving the best fit. In addition, the DEER analysis included the model-independent Tikhonov fit, which suggested additional minor components, as analyzed further in (Fig. S7).

SI Methods. ***Protein preparation and labeling.*** cMyBP-C fragment C0C2 was cloned from mouse MYBPC3 cDNA and ligated as a *BamHI-XhoI* fragment into the pET28a vector (Novagen). C0C2 contains 5 native cysteines (C1 contains 2 near the surface and C2 contains 3 that are buried), however only one native Cys (C248) is labeled by Cys-reactive probes under our labeling conditions. Site-directed mutagenesis (Stratagene) was performed to engineer a pair of Cys residues into the construct for thioreactive spin label attachment at chosen sites (S18C and C248, S169C and C248, or S440C and C248). The sites for Cys substitution were chosen because they are in β-sheets regions near the protein outer-surface in crystal and/or NMR structures of individual cMyBP-C domains (2K1M for C0, 2AVG and 3CX2 for C1, 2LHU for MyBP-C motif, and 1PD6 for C2), and the predicted interprobe distances are within the overlapping sensitivity range of FRET and DEER (~2-6 nm [2]).

The double-Cys mutant constructs were transformed into the *Escherichia coli* BL21 DE3 cell line and grown at 37 ^{o}C in LB media to an absorbance of 0.6-0.8 at 600 nm. Cells were induced with 1 mM IPTG and allowed to grow for 3 h at 37 ^{o}C. Cells were then harvested by centrifugation and lysed with lysozyme for 1 hour at 4^{o}C in 50 mM sucrose, 5 mM EDTA, 1 mM PMSF, 25 mM Tris (pH 8.0, 4^{o}C), followed by a freeze-thaw procedure in a dry ice/isopropanol bath. The lysate was treated with 2U/L DNase I and incubated with the addition of 10 mM $MgCl_2$ for 1 hour, then centrifuged at 40,000 *x g* for a total 30 minutes in two washes. The supernatant was purified using subsequent His60 Superflow resin (Clontech) and a HiPrep Sepharcryl S-100 high resolution size exclusion column (GE Healthcare Life Sciences). His_6-tagged protein was eluted with imidazole for eluting protein from His60 Superflow nickel resin, prior to size exclusion chromatography for improved C0C2 purity. Fractions containing the target protein in each column run were verified using SDS-PAGE and pooled.

Before labeling, C0C2 proteins were reduced with DTT for 60 min on ice. Excess DTT was removed using Zeba desalting columns (Pierce) in 50 mM NaCL and 50 mM Tris, pH 7.5. The protein was labeled with IAEDANS and/or FMal for TR-FRET experiments or MSL for DEER experiments. For FRET experiments, the donor dye (IAEDANS) portion was under-labeled in all samples (i.e., <30% in donor-only and donor-acceptor samples) and the acceptor dye (FMal) was used in excess to label the remaining Cys in FRET samples (i.e., in donor-acceptor samples). Excess dye was removed by dialysis in fresh buffer (50 mM NaCl, 50 mM sodium phosphate, pH 7.0, and 1 mM fresh DTT) and subsequent desalting spin columns.

Labeling efficiency was determined by UV absorbance for dye concentration and colorimetric BCA assay for protein concentration (Pierce) and by mass spectrometry (see below). For DEER and EPR experiments, the MSL reaction labeled to near completion with ~5 molar equivalents of label to Cys in C0C2, and excess MSL was removed following labeling by desalting spin columns. Electrospray mass spectrometry and EPR spin counting both showed that all samples were full spin-labeled. Experiments were performed in cMyBP-C buffer containing 100 mM NaCl, 10 mM Tris-HCl pH 7.5, 2 mM $MgCl_2$, and 0.2 mM ATP (also a suitable buffer for studies in the presence of actin). For DEER, the MSL-C0C2 samples were flash-frozen in liquid nitrogen at stored at -80 ˚C with 10% glycerol added as a cryoprotectant.

In Vitro Phosphorylation of MyBP-C. Purified cMyBP-C C0C2 was phosphorylated with the catalytic subunit of Protein kinase A (PKA, Sigma), using 0.01 units of PKA per μg of MyBP-C for 1 h at 25°C [3]. Phosphorylation status of MyBP-C was assessed by Pro-Q Diamond phosphoprotein staining followed by Sypro-Ruby protein staining (Invitrogen) or mass spectrometry. Untreated MyBP-C was unphosphorylated and was incubated for 1 h at 25 °C without PKA. To confirm that C0C2 was homogeneously unphosphorylated without PKA treatment and homogenously phosphorylated with PKA treatment, samples were additionally run on SDS-PAGE containing 50 μM Phos-tag^{TM} acrylamide (SuperSep Phos-tag^{TM}, Wako Chemicals) to analyze for differential cMyBP-C phosphorylation. The gels were run for 120 minutes at 20 mA constant current. Gels were then fixed, stained and analyzed as has previously been done for cMyBP-C phosphorylation using this method [4, 5]. The use of Phos-tag^{TM} allowed for resolving zero to four cMyBP-C phosphorylation sites. Phosphorylated species were not detected in untreated samples and samples treated with PKA were highly phosphorylated (Fig. S9), consistent with earlier results [5] using software for gel image processing.

TR-FRET Analysis. Fluorescence waveforms were acquired using a high-performance time-resolved fluorometer built in collaboration with Fluorescence Innovations, Inc., using direct waveform recording rather than the conventional method of time-correlated single-photon counting [6], which offers 10^5 times higher throughput at comparable performance. Waveforms were analyzed as described previously [7].

The observed donor-only waveform $F_{Dobs}(t)$ was fitted by a simulation $F_{Dsim}(t)$, consisting of a multiexponential decay $F_D(t)$ convolved with the instrument response function (IRF, from water light scatter),

$$F_D(t) = \sum_{i=1}^{n} A_i \exp(-t/\tau_{Di}) , \quad [S1]$$

$$F_{Dsim}(t) \int_{-\infty}^{+\infty} IRF(t-t') F_D(t') dt',$$

where τ_{Di} are donor-only fluorescence lifetimes. The best fit was obtained with $n = 3$ in Eq. 1. The waveform of donor-acceptor labeled myosin before convolution, $F_{DA}(t)$, was fitted assuming that the acceptor increases the decay rate due to energy transfer [8]. In the most general case, a distribution of donor-acceptor distances $\rho(r)$ was assumed:

$$F_{DA}(t) = \int_{-\infty}^{+\infty} \rho(R) \cdot \sum_{i=1}^{n} A_i \exp\{(-t/\tau_{Di})(1+[R_{0i}/R]^6)\} dr , \quad [S2]$$

and the observed waveform $F_{D+Aobs}(t)$ was fitted by $F_{D+Asim}(t)$:

$$F_{D+A}(t) = X_D F_D(t) + (1-X_D) F_{DA}(t), \quad [S3]$$

$$F_{D+Asim}(t) = \int_{-\infty}^{+\infty} IRF(t-t') \cdot F_{D+A}(t') dt' ,$$

where X_D is the fraction of proteins labeled only with donor.

Several functional forms of $\rho(R)$ were tested: single discrete distance (1R), two discrete distances (2R), single Gaussian (1G), and two Gaussian components (2G): The best fits (indicated by residual plots and χ^2) were consistently obtained for the 2G model,

$$\rho(r) = \frac{1}{\sigma\sqrt{2\pi}} \exp\left(-\frac{(r-R)^2}{2\sigma^2}\right), \ \sigma = \frac{FWHM}{2\sqrt{2\ln 2}} , \quad [S4]$$

where σ is the standard deviation and FWHM is the full width at half maximum of the distribution.
Each fit yielded five independent parameters of $\rho(R)$: centers R_1 and R_2, widths $FWHM_1$ and $FWHM_2$, and mol fraction X_1.

CW-EPR spectroscopy. Spin-spin distances were also determined by dipolar continuous wave (CW)-EPR, for detecting distances from 0.5 to 2.5 nm, using a Bruker E500 spectrometer at X-band (9.5 GHz) with an SHQ cavity, as described previously [9]. Spectra were acquired at 200K with a 200G field sweep to detect spectral broadening. The modulation amplitude was decreased to 1G to minimize modulation broadening, and all spectra were acquired under non-saturating conditions (0.03mW).

Modeling and preparation of the MyBP-C motif structure. The NMR structure reported for the MyBP-C motif (i.e., M-domain) only contains residues Glu315-Lys349 (PDB: 2lhu). Therefore, we constructed a structural model of the full MyBP-C motif (residues His255-Lys356). We used five methods to predict structural disorder in the motif: PONDR-FIT [10], IUPred [11], DisEMBL [12], SPINE-D [13], and ESpritz [14]. In addition, we also performed secondary structure predictions using JPRED [15] and PSIPRED [16]. By using these methods, we confirmed that residues 315-350 are structurally ordered, in agreement with NMR data. Furthermore, we found that residues His255-Glu315 are intrinsically disordered, and that this segment does not contain any significant amount of secondary structure. Based on these findings, we constructed a model of the motif. First, we generated a completely extended model of the N-terminal domain (residues His255-Glu315). To generate a truly random model of the isolated N-terminus in solution, we performed a 50-ns MD simulation of this segment at 310K. The

final structure was then attached to the NMR structure of the 3-helix bundle (residues 315-350). Residues Gly350-Lys356 were modelled as an ideal α-helix at the C-terminus of the protein. We performed an explicit solvent, 100-ns MD run at 310K to optimize the final structure. The structure at the end of this simulation was used for the production MD simulations.

The final structure at t=100 ns was used as a starting structure to simulate unphosphorylated and phosphorylated MyBP-C motif. For the phosphorylated motif, phosphoserine patches were added to serines 273, 282 and 302. Both unphosphorylated and phosphorylated proteins were solvated using TIP3P water molecules with a minimum margin of 2.5 nm between the protein and the edges of the periodic box. Na^+ and Cl^- ions were added to the system to neutralize the charge of the system and to produce a NaCl concentration of approximately 150 mM. CHARMM36 force field topologies were used for the protein, water and ions [17, 18]. We used this force field because it was recently shown that it describes well the structural dynamics of a disordered protein in solution [19].

Electrospray Ionization Mass Spectrometry. To confirm extent of labeling and phosphorylation, we used a calibrated electron-spray ionization source (ESI) to ionize the proteins and determine the associated change in mass. Labeled and unlabeled C0C2 samples at 80 μM were dialyzed in Ammonium Bicarbonate buffer (10 mM, pH 7.9 with 1 mM DTT) in order to minimize salts in the solution that may affect the protein charge. A typical sample injected into the spectrometer was 10 μL with consistent results. Mixtures of unlabeled and labeled proteins were used to assess the fraction of labeled protein and analysis of peaks was performed using the Analyst QS program.

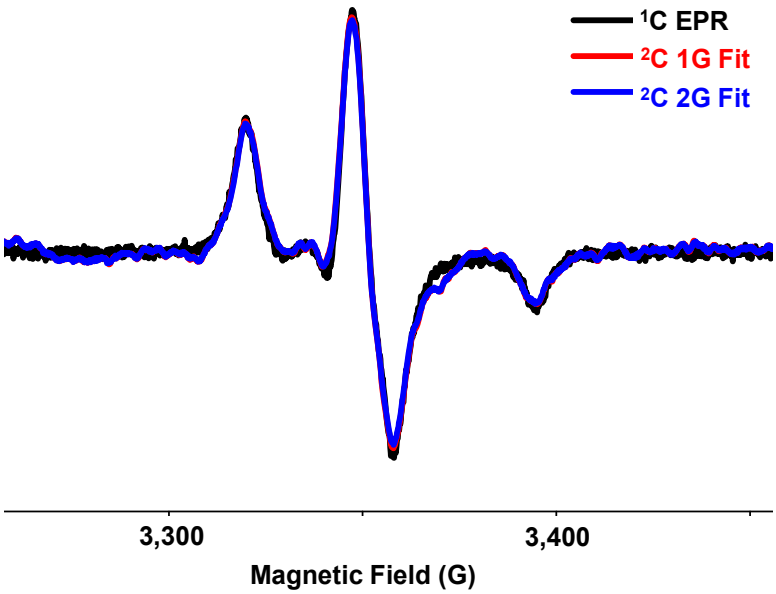

Fig. S1. Dipolar EPR of C0C2 S16C.C248 shows that there is a small but significant difference in linewidth of ~0.6G, between singly-labeled (non-interacting in black, ^{1}Cys EPR) C0C2 and doubly-labeled (red, blue) C0C2 with spin labels in the C1 domain. Singly- and doubly- labeled C0C2 spectra were compared in peak broadening and fit to 1 (red, ^{2}Cys 1G Fit) and 2 (blue, ^{2}Cys 2G Fit) Gaussians, without significant improvement of the fit, with the conclusion that distances much shorter than 2.5 nm are not present in the sample. See Table S1 for distance measurements of each fit.

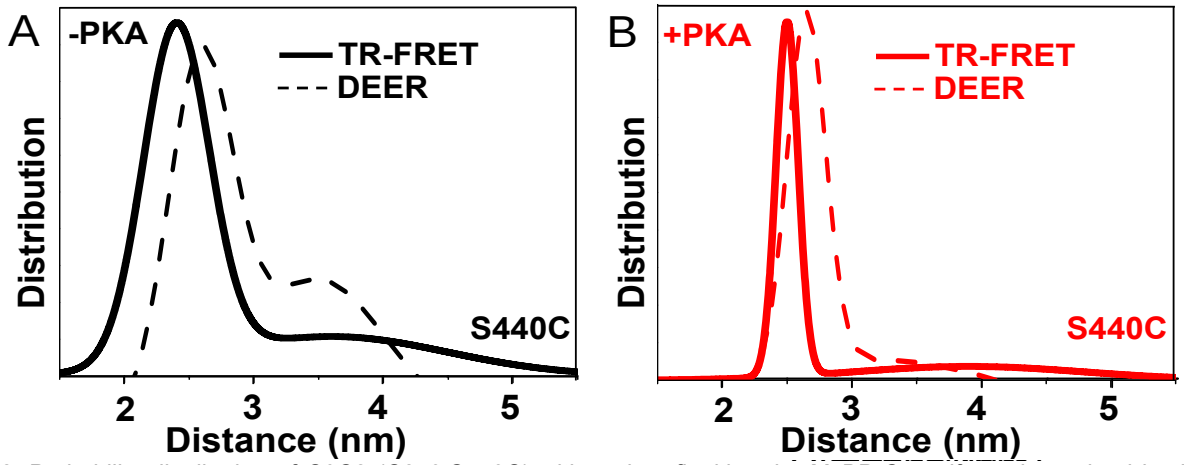

Fig. S2. Probability distribution of C0C2 (C248.S440C) with probes flanking the MyBP-C motif, as determined by **(A)** TR-FRET (black) or DEER (dashes) and **(B)** the effect of phosphorylation by PKA treatment using TR-FRET (red) or DEER (red dashes). All were fit to a two-Gaussian distribution with centers at the mean distance of each peak. The Gaussian's full-width at half-maximum height (FWHM) relates to the level of labeled C0C2 disorder.

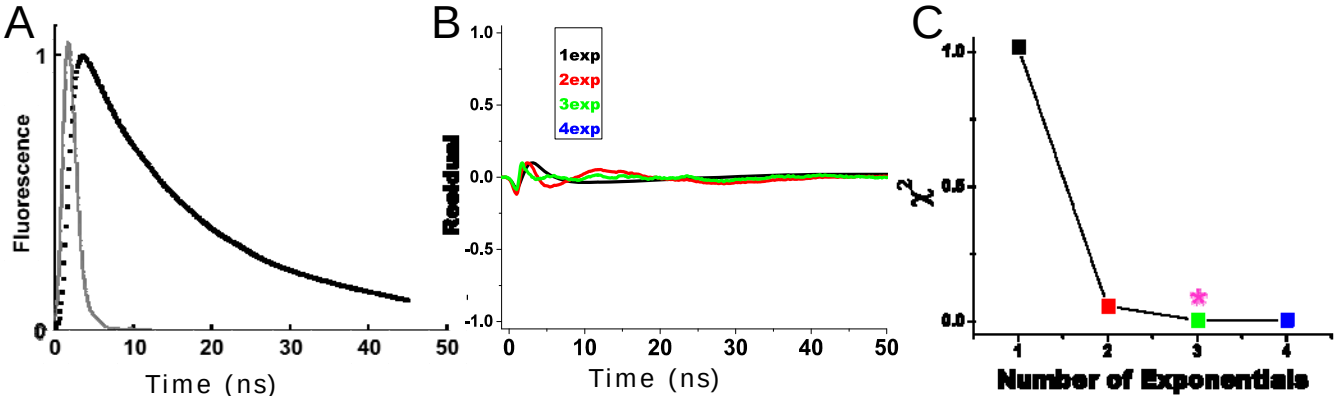

Fig. S3. Details of FRET analysis for donor-only data used in Fig. 4. **(A)** Time-resolved (TR) fluorescence data of donor-only C248.S440C-C0C2 (thick waveform) and Instrument Response Function (IRF, thin waveform). **(B)** Donor-only lifetimes of labeled C0C2 for FRET were analyzed by 1, 2, 3, and 4 –exponentials in the fit (Eq S1). Residuals of each fit (data minus fit) are plotted. The 4-exponential fit is indistinguishable from the 3-exponential fit. **(C)** χ^2 values for the fits shown in B, showing clearly that the 3-exponential fit was better than 2, and that 4 exponentials gave no further improvement. Thus the 3-exponential analysis was used.

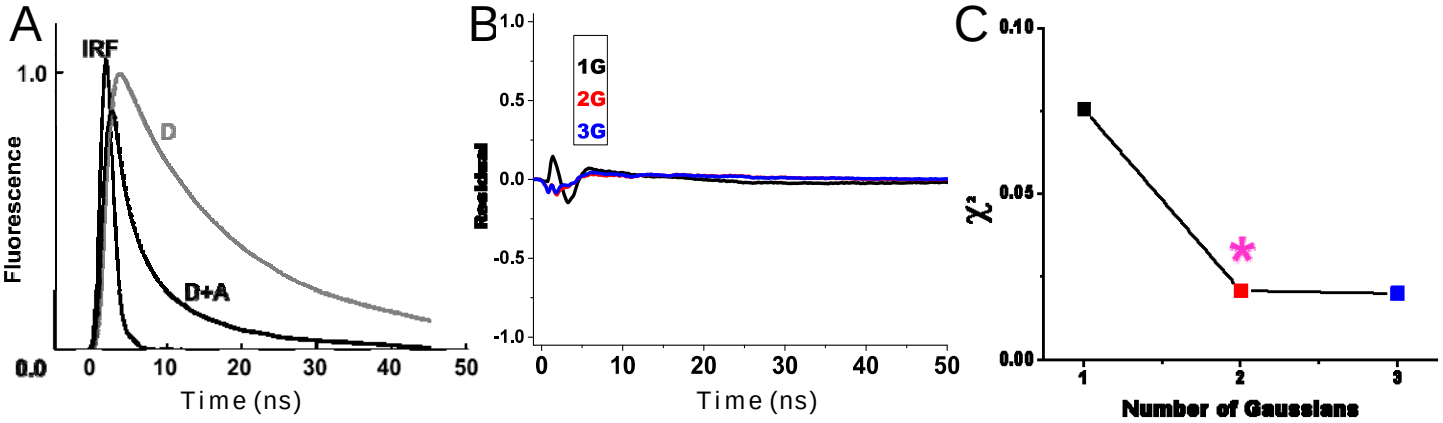

Fig. S4. Details of FRET analysis for data in Fig. 4. **(A)** TR-fluorescence of C248.S440C-C0C2. Fluorescence waveforms of both donor (*D*) and donor-acceptor (*D* + *A*), and the IRF. **(B)** Residuals from fits for donor-acceptor data in A, assuming 1, 2, and 3 Gaussian distance distributions (Eq S2-S4), showing (data – fit)/(maximum fit value). **(C)** χ^2 values for the fits shown in B, showing clearly that the 2-Gaussian fit was better than 1, and that 3 Gaussians gave no further improvement. Thus the 2-Gaussian analysis was used.

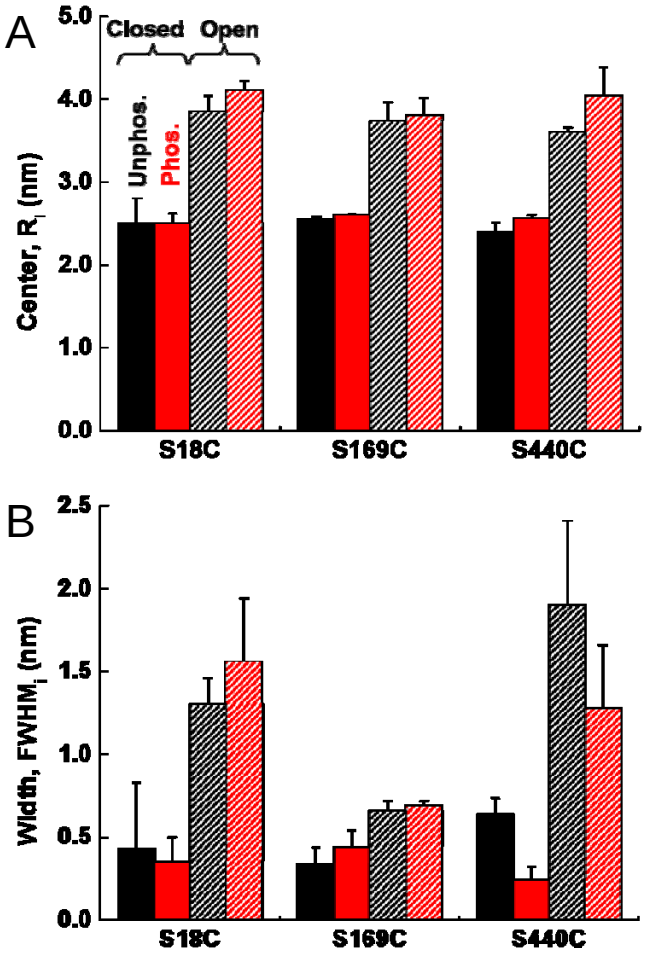

Fig. S5. Results of independent fits (Eqs. S2-S4, *n* = 3) for unphosphorylated (black) and phosphorylated (red) C0C2, assuming two Gaussian distributions: closed state (solid) and open state (striped). Error bars are SEM (*n* = 3). **(A)** Center distances and **(B)** widths of the distribution for each of the 3 intra-molecular probe pairs (in PAL, C1, or motif) to C248 in C1 are shown in the bars.

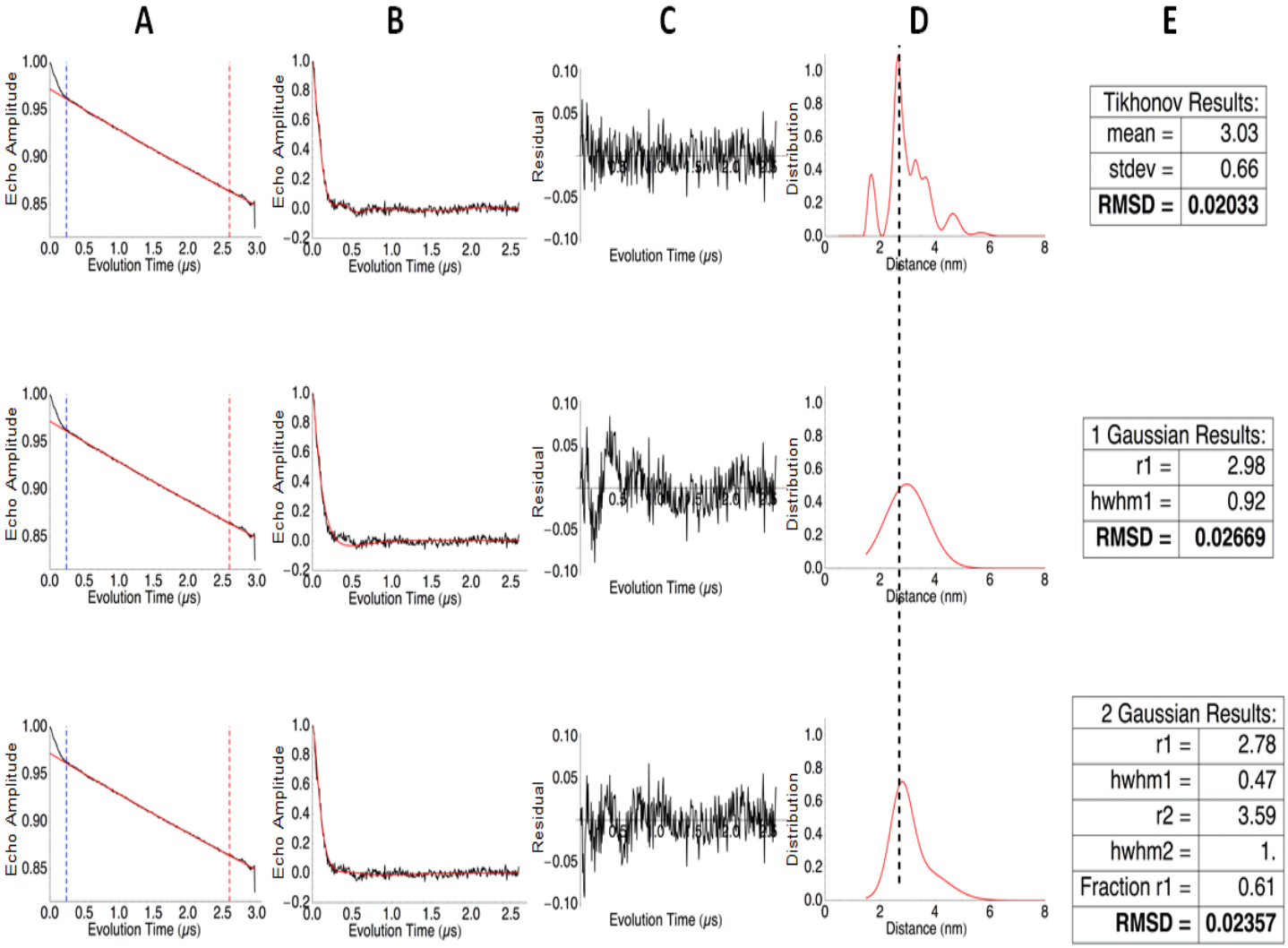

Fig. S6. Raw DEER data and analysis of data shown in Fig. 2, illustrating how different models were evaluated. **(A)** Time-dependent DEER waveform (echo amplitude) of doubly spin-labeled C0C2 (raw data shown in black) was background-subtracted (background shown in red) by a fitting a portion of the spectrum (blue to red dotted lines at ~0.25 to 2.6 μs of the evolution time) to an exponential decay, assuming a 3D homogeneous distribution of spins. **(B)** Normalized DEER waveform (black) and fit (red) to Tikhonov, 1 Gaussian, or 2 Gaussians (red lines: top, middle, bottom, respectively). **(C)** Residuals from fits. **(D)** Distance distributions from fits. **(E)** Statistics from fits. More detailed illustration of fitting procedure is shown in *Supplementary Index,* Fig. S7.

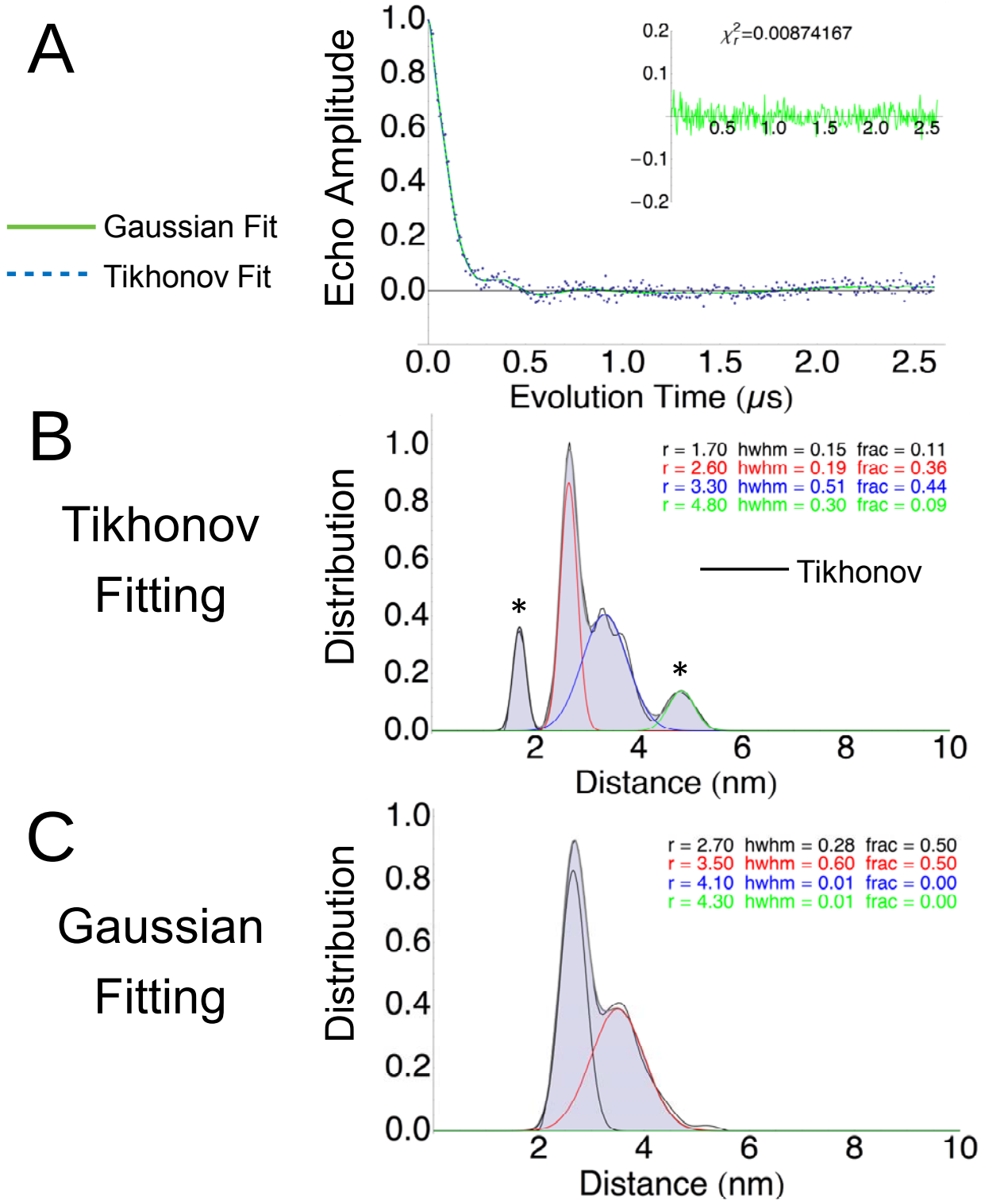

Fig. S7. Spin-echo DEER waveforms of doubly spin-labeled C0-C2 were analyzed, with 2-Gaussians providing the best fit for the dominant spectral features. However, direct fitting of DEER waveforms to Gaussian models are easily trapped in unrealistic solutions due to experimental artifacts and deviations from ideal background components, therefore fits were derived initially from a model-independent Tikhonov fit then further analyzed for Gaussian populations. Shown above is the **(A)** fitting of the DEER decay with Gaussian fit residual (inset). Reduced Chi-squared (χ^2) for the Gaussian fit was computed using the Tikhonov profile as a reference. **(B)** Shown in the middle panel is the Gaussian fit (shaded envelope and colored sub-populations) of the Tikhonov distribution (thin black line) having additional features not in the shaded region of the distribution. The * marked populations are deemed to be artifacts via comparison with CW dipolar experiments (short distance peak) and through the use of the background correction validation tool provided in DeerAnalysis 2013 (long distance peak). **(C)** Shown below is the resulting Gaussian populations (shaded region) derived from Tikhonov fit (thin black line) of DEER waveforms after artifact populations were removed.

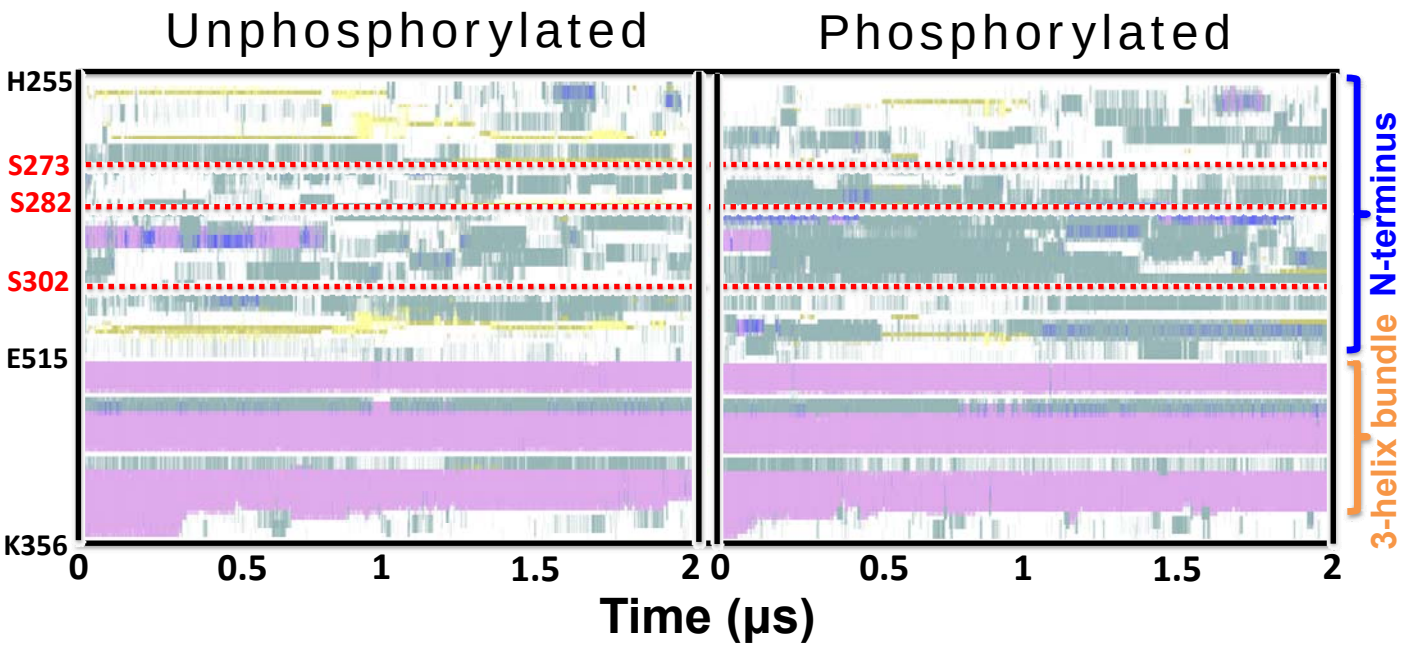

Fig. S8. Time-dependent secondary structure changes of unphosphorylated and phosphorylated MyBP-C motif (i.e., M-domain). The location of the phosphorylation sites is shown as dashed lines in red. The keys on the left indicate the location of the unstructured N-terminus (residues His255-Glu315) and the 3-helix-bundle (residues Glu315-Lys349). Secondary structure is colored as α-helix (pink), 310-helix (blue), β-strand (yellow) turn (cyan), and coil (white).

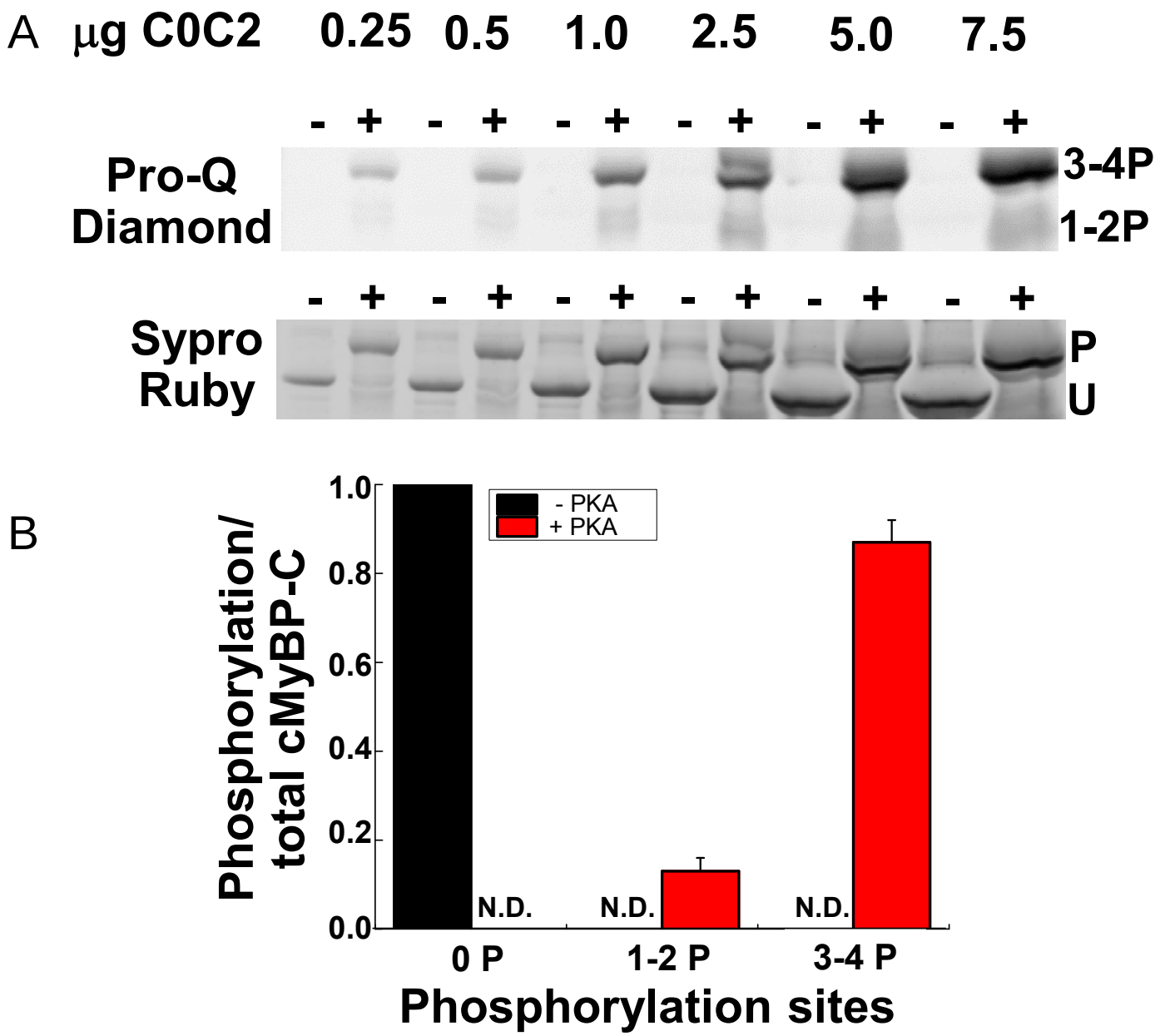

Fig. S9. (A) Phosphorylation of C0C2 detected by phosphate affinity SDS-PAGE (containing Phos-Tag™ acrylamide; Wako Chemicals, Osaka, Japan). The same gel was stained with Pro-Q Diamond (top) or Sypro Ruby (bottom) to resolve individual phosphospecies due to PKA treatment. Untreated C0C2 (-) had no detectable phosphorylation in Pro-Q Diamond stain and migrated lower than PKA-treated samples (+) after staining with Sypro Ruby. PKA-treated C0C2 (+) was nearly homogenously phosphorylated at 3-4 phosphorylation sites, with faint detection of 1-2 phosphorylation sites. **(B)** Relative intensity of phosphospecies with no phosphorylation, 1-2 sites, or 3-4 sties phosphorylated (N.D. = not detectable), corrected for protein load.

TABLE S1: Fits for dipolar EPR of C0C2 S169C.C248 within the C1 domain does not exhibit strong evidence for distances with peak centers shorter than 2.5 nm.

Gaussians	Unbroadened	X_1 (mol)	R_1 (nm)	X_2 (mol)	R_1 (nm)	χ^2
1	0.05	0.95	2.8 ± 2.1	-	-	1.5×10^{-5}
2	0.08	0.74	2.6 ± 0.7	0.18	1.3 ± 1.5	1.4×10^{-5}

Dipolar EPR (i.e., CW-EPR) measurements show that there is a difference in the linewidth of ~0.6G, which is small but significant ($p<0.05$). These distances have fairly high disorder, >2 nm, because these distances are at the sensitivity limit for dipolar EPR, and in a much better distance range for DEER and TR-FRET spectroscopic approaches, with sensitivity in the 2-6 nm range.

TABLE S2: Distance measurements for C0C2 from S169C to C248 of the C1 domain.

Spectroscopy	Mean Distance (nm)	Deviation from Mean (nm)	Mole Fraction
NMR	2.3	0.2	1.0
X-ray	2.3	0.1	1.0
TR-FRET	2.6	0.3	0.7
DEER	2.6	0.6	0.7

C1 domain NMR and crystal structure measurements are Cα-Cα distances using computer software (PDB: 2AVG and 3CX2, respectively), whereas TR-FRET and DEER measurements are from fitted spectra of labeled-C0C2 with probes across the C1 domain.

TABLE S3: Likelihood of protein-protein interaction site locations within the MyBP-C motif

AA	Residue	Probability	Prediction
E	315	0.052	N
D	316	0.085	N
V	317	0.000	-
W	318	0.993	P
E	319	0.974	P
I	320	0.450	N
L	321	0.000	-
R	322	0.916	P
Q	323	0.361	N
A	324	0.105	N
P	325	0.302	N
P	326	0.054	N
S	327	0.033	N
E	328	0.212	N
Y	329	0.889	P
E	330	0.126	N
R	331	0.418	N
I	332	0.990	P
A	333	0.000	-
F	334	0.094	N
Q	335	0.981	P
H	336	0.986	P
G	337	0.961	P
V	338	0.995	P
T	339	0.995	P
D	340	0.994	P
L	341	0.991	P
R	342	0.995	P
G	343	0.463	N
M	344	0.000	-
L	345	0.985	P
K	346	0.975	P
R	347	0.866	P
L	348	0.966	P
K	349	0.038	N

Protein-protein binding site predictions within MyBP-C motif (i.e., M-domain) using cons-PPISP [20]. The consensus method is based on protein structure, amino acid charge, position-specific sequence profiles, and solvent accessibilities of each residue and its spatial neighbors, based on known structures of protein complexes. P: positively predicted residue for interactions, N: negatively predicted residue for interactions, -: buried residue; 0: low probability of protein-protein interaction site, 1: high probability of protein-protein interaction site**.**

REFERENCES

1. Ratti, J., et al., *Structure and interactions of myosin-binding protein C domain C0: cardiac-specific regulation of myosin at its neck?* J Biol Chem, 2011. 286(14): p. 12650-8.
2. Jeschke, G., *DEER distance measurements on proteins.* Annual review of physical chemistry, 2012. 63: p. 419-46.
3. Rybakova, I.N., M.L. Greaser, and R.L. Moss, *Myosin binding protein C interaction with actin: characterization and mapping of the binding site.* J Biol Chem, 2011. 286(3): p. 2008-16.
4. Kinoshita, E., et al., *Phosphate-binding tag, a new tool to visualize phosphorylated proteins.* Mol Cell Proteomics, 2006. 5(4): p. 749-57.
5. Copeland, O., et al., *Analysis of cardiac myosin binding protein-C phosphorylation in human heart muscle.* Journal of molecular and cellular cardiology, 2010. 49(6): p. 1003-11.
6. Muretta, J.M., et al., *High-performance time-resolved fluorescence by direct waveform recording.* Rev Sci Instrum, 2010. 81(10): p. 103101.
7. Li, J., et al., *Structural and functional dynamics of an integral membrane protein complex modulated by lipid headgroup charge.* J Mol Biol, 2012. 418(5): p. 379-89.
8. Kast, D., et al., *Phosphorylation-induced structural changes in smooth muscle myosin regulatory light chain.* Proc Natl Acad Sci U S A, 2010. 107(18): p. 8207-12.
9. Klein, J.C., et al., *Actin-binding cleft closure in myosin II probed by site-directed spin labeling and pulsed EPR.* Proc Natl Acad Sci U S A, 2008. 105(35): p. 12867-72.
10. Xue, B., et al., *PONDR-FIT: a meta-predictor of intrinsically disordered amino acids.* Biochim Biophys Acta, 2010. 1804(4): p. 996-1010.
11. Dosztanyi, Z., et al., *IUPred: web server for the prediction of intrinsically unstructured regions of proteins based on estimated energy content.* Bioinformatics, 2005. 21(16): p. 3433-4.
12. Linding, R., et al., *Protein disorder prediction: implications for structural proteomics.* Structure, 2003. 11(11): p. 1453-9.
13. Zhang, T., et al., *SPINE-D: accurate prediction of short and long disordered regions by a single neural-network based method.* J Biomol Struct Dyn, 2012. 29(4): p. 799-813.
14. Walsh, I., et al., *ESpritz: accurate and fast prediction of protein disorder.* Bioinformatics, 2012. 28(4): p. 503-9.
15. Cuff, J.A. and G.J. Barton, *Application of multiple sequence alignment profiles to improve protein secondary structure prediction.* Proteins, 2000. 40(3): p. 502-11.
16. Jones, D.T., *Protein secondary structure prediction based on position-specific scoring matrices.* J Mol Biol, 1999. 292(2): p. 195-202.
17. Best, R.B., et al., *Optimization of the additive CHARMM all-atom protein force field targeting improved sampling of the backbone phi, psi and side-chain chi(1) and chi(2) dihedral angles.* J Chem Theory Comput, 2012. 8(9): p. 3257-3273.
18. MacKerell, J., A. D., et al., *All-atom empirical potential for molecular modeling and dynamics studies of proteins.* J Phys Chem B, 1998. 102: p. 3586-3616.
19. Espinoza-Fonseca, L.M. and A. Kelekar, *High-resolution structural characterization of Noxa, an intrinsically disordered protein, by microsecond molecular dynamics simulations.* Mol Biosyst, 2015. 11(7): p. 1850-6.
20. Chen, H.L. and H.X. Zhou, *Prediction of interface residues in protein-protein complexes by a consensus neural network method: Test against NMR data.* Proteins-Structure Function and Bioinformatics, 2005. 61(1): p. 21-35.